Research Square

Preprints are preliminary reports that have not undergone peer review.
They should not be considered conclusive, used to inform clinical practice,
or referenced by the media as validated information.

Full-Length Transcriptome Profiling of Wheat to Spot Blotch across Tissues and Genotypes

Shuang Liang
Shandong Agricultural University
Xinyu Wan
Shandong Agricultural University
Chunting Wang
Shandong Agricultural University
Yuanrui Zhu
Shandong Agricultural University
Jian Shen
Shandong Agricultural University
Yinguang Bao
Shandong Agricultural University
Haitao Cui
Shandong Agricultural University
Xingfeng Li
lixf@sdau.edu.cn

Shandong Agricultural University

Research Article

Keywords: Spot blotch, Bipolaris sorokiniana, Common wheat, Susceptibility

Posted Date: November 25th, 2026

DOI: https://doi.org/10.21203/rs.3.rs-11622026/v1

License: This work is licensed under a Creative Commons Attribution 4.0 International License.
Read Full License

Additional Declarations: No competing interests reported.

Full-Length Transcriptome Profiling of Wheat to Spot Blotch across Tissues and Genotypes

Shuang Liang[1,3,†], Xinyu Wan[1,2,†], Chunting Wang[1,2], Yuanrui Zhu[1,2], Jian Shen[2], Yinguang Bao[1,2], Haitao Cui[1,3], Xingfeng Li[1,2*]

[1] State Key Laboratory of Wheat Improvement, Shandong Agricultural University, Tai'an, Shandong 271000, China

[2] Agronomy College, Shandong Agricultural University, Tai'an, Shandong 271000, China

[3] College of Plant Protection, Shandong Agricultural University, Tai'an, Shandong 271000, China

[†] These authors contributed equally to this work.

* Corresponding author:

Xingfeng Li, Phone: 86-538-8246821, Fax: 86-538-8242226, E-mail: lixf@sdau.edu.cn

Abstract

Background

Spot blotch, caused by the hemibiotrophic fungus *Bipolaris sorokiniana*, is a major constraint on global wheat production. Although several resistance genes and QTLs have been identified, the transcriptional architecture of both resistance and susceptibility-particularly its organ specificity and post-transcriptional complexity-remains poorly resolved. Full-length transcriptome profiling across multiple tissues and genetic backgrounds carrying different resistance loci is therefore required to distinguish passive failure of defence from active, pathogen-exploitable susceptibility programmes.

Results

In this study, we generated the first multi-tissue Oxford Nanopore full-length transcriptome atlas of the wheat-*B. sorokiniana* interaction by sequencing leaves, leaf sheaths and glumes of the resistant-susceptible pair ZS54 (R)/ZS57 (S) and integrating an independent leaf transcriptome dataset from a second pair (ZS31/ZS3, R/S) that carries different resistance loci. High-quality long-read data identified 6,996 novel genes and 11,072 novel isoforms, many of which were enriched in plant-pathogen interaction pathways. Differential expression analysis revealed a conserved susceptibility signature characterised by systemic down-regulation of photosynthesis (Calvin cycle, antenna proteins and chloroplast components) accompanied by hyperactivation of Mitogen-activated protein kinase (MAPK) signalling, plant-pathogen interaction, phenylpropanoid and glutathione metabolism, and cell-wall

catabolism. Tissue-resolved responses were distinct: sheaths emphasised cell-wall reinforcement and redox processes, leaves showed carbon mobilisation and lipid degradation, and glumes activated secondary metabolism and energy pathways. Weighted gene co-expression network analysis (WGCNA) identified organ-specific modules tightly correlated with disease severity and nominated hub genes encoding a xyloglucan endotransglucosylase/hydrolase, a pentatricopeptide-repeat protein and a PPPDE thiol peptidase. Comparison confirmed that, despite the different chromosomal locations of the resistance loci, both resistant lines (ZS54 and ZS31) exhibited coordinated transcriptional reinforcement of chloroplast structure, photosynthetic machinery and related stress-response processes under fungal challenge. In contrast, photosynthetic collapse and unproductive defence hyperactivation, including HR/ROS programmes that benefit the necrotroph, were shared susceptibility features, while residual flavonoid and structural capacity modulated quantitative disease severity.

Conclusions

Although the resistance loci of these two pairs of materials are located on different chromosomes, the core transcriptional programmes are largely shared. Resistant genotypes maintain coordinated reinforcement of chloroplast structure and photosynthetic machinery, consistent with a protective acclimation that preserves tissue integrity, whereas susceptible genotypes exhibit photosynthetic collapse accompanied by unproductive defence hyperactivation. Residual flavonoid capacity further modulates quantitative disease severity. The isoform-resolved, multi-organ dataset expands the candidate pool of susceptibility determinants and supplies concrete

65 molecular targets-protection of chloroplast integrity, calibration of cell-death pathways,

66 and maintenance of flavonoid metabolism-for breeding durable resistance.

67 **Keywords**: Spot blotch, *Bipolaris sorokiniana*, Common wheat, Susceptibility

68

1 Introduction

As one of the primary staple foods, wheat (*Triticum aestivum* L.) supplies approximately 20% of the global population's caloric intake [1]. Its production, however, is increasingly constrained by both abiotic and biotic stresses. Among the latter, fungal diseases-powdery mildew, rusts, Fusarium head blight, and the leaf-spotting complex-are the principal culprits, collectively eroding both grain quantity and quality [2].

Wheat leaf blight encompasses a group of destructive foliar diseases characterized by leaf spots and blights caused by multiple pathogenic fungi. The four most economically important leaf blight pathogens currently posing the greatest threat to wheat yield and grain quality are *Pyrenophora tritici-repentis* (causing tan spot, TS), *Zymoseptoria tritici* (causing *Septoria tritici* blotch, STB), *Parastagonospora nodorum* (causing *Septoria nodorum* blotch, SNB), and *Bipolaris sorokiniana* (causing spot blotch, SB) [3]. Spot blotch is globally distributed, with recurrent and highly damaging epidemics occurring in the Gangetic Plains of South Asia, southern China, and the Yangtze River Basin, where it has become a major bottleneck to wheat production [4]. Regional surveys in 2025 revealed a continuing expansion of the affected area in the Yangtze River Basin. Driven by climate warming and the intensification of cropping systems, the geographic range and epidemic frequency of spot blotch are projected to increase further, posing a sustained and escalating threat to global wheat yield and grain quality [5, 6].

Symptoms of spot blotch on infected leaves-particularly the lower, older leaves-

initially appear as small brown lesions (1 mm in diameter) surrounded by yellow halos. As the disease progresses, these lesions rapidly expand and coalesce into elliptical or irregular large spots with necrotic centers, ultimately causing widespread leaf necrosis, premature senescence, and complete loss of photosynthetic function. After heading, the pathogen can also infect glumes and grains, leading to head blight and seed contamination [4].

Host resistance represents the most economical and sustainable core strategy for managing *B. sorokiniana*. Wheat resistance to spot blotch is conferred by both major resistance genes (*Sb* series) and quantitative trait loci (QTLs) [4, 7]. To date, five major genes have been mapped: *Sb1* on 7DS tightly linked to the broad-spectrum *Lr34/Yr18/Pm38* locus encoding an ABC transporter [8]; *Sb2* on 5BL co-locating with *Tsn1* and *PmG25* [9, 10]; *Sb3* on 3BS in line '621-7-1' [11]; *Sb4* on 4BL in cultivars 'Zhongyu 1211' and 'GY17'[12]; and *SbWE35* on 4BL with substantial overlap *Sb4* intervals[13]. These genes act via classical gene-for-gene or inverse gene-for-gene mechanisms, while the susceptibility gene *Tsn1* (5BL) interacts with the effector *ToxA*, and its loss-of-function allele enhances resistance [7, 14]. GWAS and high-density SNP arrays have further identified multiple QTLs and candidates (e.g., *Qsb.hebau*-1BL and *TaNADPO*), underscoring polygenic regulation [15–18]. However, the transcriptional regulatory mechanisms underlying these genes and QTLs remain largely unclear.

Nevertheless, resistance conferred by major R genes is frequently overcome by pathogen evolution and is therefore often short-lived. An increasingly attractive complementary strategy targets the opposite side of the interaction-susceptibility (S)

genes, which are host genes required for successful pathogen infection, colonization, or proliferation. Resistance mediated by loss-of-function mutations in S genes is frequently durable and broad-spectrum [19–22]; for example, CRISPR editing of the wheat S gene *TaPsIPK1*, which is hijacked by a stripe-rust effector, conferred broad-spectrum resistance without yield penalties [23]. Importantly, spot blotch pathosystem already provides a natural paradigm for this concept: the susceptibility gene *Tsn1* (5BL) interacts with the fungal effector ToxA, and its loss-of-function allele enhances resistance [7, 14], indicating that susceptibility here is not merely the absence of resistance but an active, genetically programmed state[24, 25]. Understanding the transcriptional reprogramming that accompanies this active susceptible state-particularly in severely affected genotypes such as ZS57-is therefore essential for identifying new S-gene candidates and durable resistance alleles.

In the spot blotch pathosystem, susceptibility is not simply the absence of resistance but an active, genetically programmed process. Understanding the transcriptional reprogramming that occurs after infection in susceptible genotypes such as ZS57 is therefore essential. To systematically elucidate the locus-specific and conserved defense mechanisms against spot blotch, we generated multi-tissue full-length transcriptome data-spanning leaves, glumes, and leaf sheaths across multiple time points-from the resistant-susceptible wheat pair ZS54 (R) and ZS57 (S). To validate key expression patterns and ensure the robustness of our findings, these profiles were integrated with existing long-read leaf transcriptome data from an independent resistant-susceptible pair, ZS31 (R) and ZS3 (S). This dual-population strategy

establishes a comprehensive transcriptional architecture of wheat immunity against spot blotch across diverse tissues and developmental stages.

2 Materials and methods

2.1 Plant materials

This study used four sister wheat lines with contrasting disease responses from the Zhouyuan9369 and SN670 germplasm lines: the resistant genotypes ZS54 and ZS31, and the susceptible genotypes ZS57 and ZS3. The primary experimental materials were planted in the experimental field of Shandong Agricultural University under conventional water and fertilizer management. Typical diseased leaves were surface-sterilized and plated on PDA for pathogen isolation. Pure cultures were obtained by single-spore isolation and identified as *B. sorokiniana* on the basis of morphological characteristics combined with ITS and Gpd1 sequence analysis. A secondary independent pair of wheat cultivars, ZS31 and ZS3, was utilized for cross-validation. Detailed sequencing statistics, quality controls, and read-length distributions for the ZS31 (R)/ZS3 (S) libraries are provided in Supplementary Table S2 and Supplementary Figure S2 and Figure S3.

2.2 RNA extraction and sequencing

Total RNA was extracted from leaves, glumes, and sheaths of both resistant and susceptible wheat plants at the appropriate time point after disease onset. Samples were immediately frozen in liquid nitrogen and ground into a fine powder using a mortar and pestle. Total RNA was then isolated using the TIANGEN RNAprep Pure Plant Kit according to the manufacturer's instructions. RNA concentration and purity were assessed with a NanoDrop 2000 spectrophotometer, and RNA integrity was evaluated by agarose gel electrophoresis.

Full-length mRNA was reverse-transcribed using the SuperScript IV First-Strand Synthesis System (Invitrogen). The cDNA was amplified for 14 PCR cycles with LongAmp Taq DNA Polymerase (New England Biolabs, Ipswich, MA, USA). The PCR products underwent DNA repair and end-repair with the NEBNext FFPE DNA Repair Mix (New England Biolabs), followed by adapter ligation using T_4 DNA ligase (New England Biolabs). Libraries were purified with Agencourt AMPure XP beads per the ONT protocol and sequenced on a FLO-MIN109 flow cell using the PromethION platform at Benagen Technology Co., Ltd. (Wuhan, China).

2.3 Read processing and differential gene expression analysis

Raw Oxford Nanopore sequencing reads were processed as follows. Reads with an average Phred quality score ≤ 7 or a read length ≤ 50 bp were discarded using NanoFilt v2.8.0 and SeqKit v0.12.0. Full-length cDNA molecules in the filtered dataset were identified, strand-oriented, and adapter-trimmed using Pychopper v2.4.0. The resulting full-length cDNA sequences were mapped to the IWGSC RefSeq v2.1 wheat reference genome using minimap2 v2.17-r941. Alignment statistics were subsequently generated using Samtools v1.11.

Non-redundant transcript sets were generated from full-length cDNA sequences using Pinfish v0.1.0. The consensus sequences were compared with known transcripts in the reference genome using gffcompare to identify novel genes and novel transcripts. Coding sequences (CDS) of the novel transcripts were predicted using TransDecoder v5.5.0.

Transcript and gene statistics were summarized for all, known, and novel

categories. Transcript density across the genome was calculated and visualized as density distribution plots using the R package circliz.

Transcript-level quantification of uniquely mapped reads was performed using IsoQuant v 3.2. Gene-level quantification was conducted using featureCounts. Principal component analysis (PCA) and clustering analyses were carried out in the R environment. Differential expression analysis was performed with DESeq2 using the thresholds of adjusted P-value (padj) < 0.05 and absolute $\log_2$ fold change ($|\log_2 FC|$) > 1. Transcripts were clustered according to their expression patterns across different samples; conversely, samples were clustered based on the expression patterns of transcripts.

2.4 Functional enrichment analysis

Gene Ontology (GO) enrichment analysis was performed to investigate the functional roles of the differentially expressed genes (DEGs) in the categories of biological process (BP), molecular function (MF), and cellular component (CC). GO terms with an adjusted P-value (padj) < 0.001 were considered significantly enriched. Kyoto Encyclopedia of Genes and Genomes (KEGG) pathway enrichment analysis was conducted using the KEGG database. The DEGs were mapped onto known signaling and metabolic pathways, and enrichment significance was evaluated using a hypergeometric test with multiple-testing correction. The enriched GO terms and KEGG pathways were interpreted in the context of host defense responses, metabolic reprogramming, and susceptibility to spot blotch in wheat.

2.5 Weighted gene co-expression network analysis

To identify functional gene modules and core regulatory networks associated with spot blotch resistance phenotypes across different tissues and genetic backgrounds, weighted gene co-expression network analysis (WGCNA) was performed using the WGCNA package (version 1.69) in R [26]. The filtered, normalized gene expression matrix along with the corresponding phenotypic datasets served as input files. Specifically, based on their resistance performance, samples from resistant and susceptible materials were assigned trait values of 0 and 1, respectively, and module eigengene–trait correlations were calculated separately for the leaf sheath, leaf, and glume.

Briefly, an appropriate soft-thresholding power (β) was calculated based on the scale-free topology criterion to ensure a scale-free network distribution. Pearson's correlation matrices between all gene pairs were calculated and transformed into an adjacency matrix, followed by conversion into a topological overlap matrix (TOM). Modules were identified using hierarchical clustering and the dynamic tree-cut algorithm, with a minimum module size set to 30 genes and a merge cut height for similar modules. Pearson correlation coefficients between module eigengenes (MEs) and target phenotypes were computed to identify core modules significantly associated with disease resistance or susceptibility traits. To pinpoint key drivers within these core modules, network connections were exported, and hub genes were visualized and screened using Cytoscape software based on edge weight and connectivity metrics.

2.6 Quantitative real-time reverse transcription PCR (qRT-PCR) analysis

Total RNA (1 μg) was reverse-transcribed into first-strand cDNA using the HiScript IV RT SuperMix for qPCR (+gDNA wiper) (Vazyme, Nanjing, China) according to the manufacturer's instructions. Quantitative PCR was performed using the SupRealQ MLtra Hunter SYBR qPCR Master Mix (U+) on a Bio-Rad CFX Opus 96 real-time PCR system. Each 20 μL reaction mixture contained 10 μL of SYBR Green Master Mix, 1 μL of each gene-specific primer (10 μM), and 2 μL of diluted cDNA template. The thermal cycling program consisted of an initial denaturation at 95°C for 30 s, followed by 40 cycles of amplification at 95°C for 10 s and 60°C for 30 s. A melting curve analysis was subsequently performed from 60°C to 95°C to verify primer specificity. The elongation factor 1-alpha (EF1A1) gene was used as the internal reference, and relative expression fold changes were calculated using the $2^{-\Delta\Delta Ct}$ comparative cycle threshold method. All reactions were performed in triplicate for each sample.

Result

3.1 ZS54, ZS31, and ZS57 and ZS3 exhibit different spot blotch resistance levels

Before the jointing stage, leaves of all four materials remained free of visible symptoms. At jointing, the susceptible (S) lines ZS57 and ZS3 developed oval lesions with yellow halos on basal leaves; these rapidly expanded into large necrotic patches, leading to premature senescence and spread to upper leaves, sheaths and, after heading, to glumes (Fig. 1a, b, e, f). In contrast, the resistant (R) lines ZS54 and ZS31 showed no lesions on leaves or spikes throughout the season (Fig. 1c, d, g, h). These plants

maintained a consistently healthy phenotype with normal, spotless leaves and completely unblemished (Fig. 1c, g), non-discolored spikes and glumes(Fig. 1d, h), confirming their robust immunity to the pathogen.

Furthermore, in the F_2 population derived from the cross between ZS54 and ZS57, the segregation ratio of resistant to susceptible individuals fitted a 1:3 ratio, consistent with monogenic inheritance. Preliminary marker-based mapping analysis indicated that the locus co-localized with *Sb3* [11] (Table S1). In contrast, the F_2 progeny of ZS31 × ZS3 exhibited a 3:1 resistant-to-susceptible segregation ratio, likewise indicating single-gene control, and the resistance gene was mapped to the same chromosomal interval as *Sb4* [12] (Table S1). So, the disease-resistant loci of these two pairs of materials are located on different chromosomes.



Fig. 1 Symptom phenotypes of spot blotch in wheat varieties with contrasting resistance. (a-b) Symptoms on leaves and glumes of the susceptible variety ZS3. (c-d) Resistant variety ZS31. (e-f) Susceptible variety ZS57. (g-h) Resistant variety ZS54. (i-k) Sheath, leaf, and glume from ZS57. Scale bars = 1 cm.

3.2 Sequencing, novel genes and isoforms identified by ONT sequencing

Six tissue samples (leaf, sheath, and glume) from ZS54 and ZS57, each with three

biological replicates, were sequenced on the Oxford Nanopore PromethION platform. After filtering, 101,160,491 clean reads (85 Gb) were obtained, with average read lengths of 810-1021 nt, mapping rates of 93.9-99.5 %, and N50 of ~1 394 bp, indicating high data quality. Reads were mapped to the IWGSC RefSeq v2.1 reference genome.

In total, 80,555 genes and 101,298 transcripts were identified, of which 6 996 genes and 11,072 isoforms were novel (Fig. 2a, b). Novel transcripts contributed substantially to plant-pathogen interaction pathways (Fig. 2c). Transcriptome-wide density profiling showed that novel transcripts accounted for 7.49 % of signal in high-density regions and were enriched in subtelomeric zones (Fig. 2d). These results demonstrate that ONT long-read sequencing efficiently expands the wheat transcriptome annotation, particularly for pathogen-response genes.

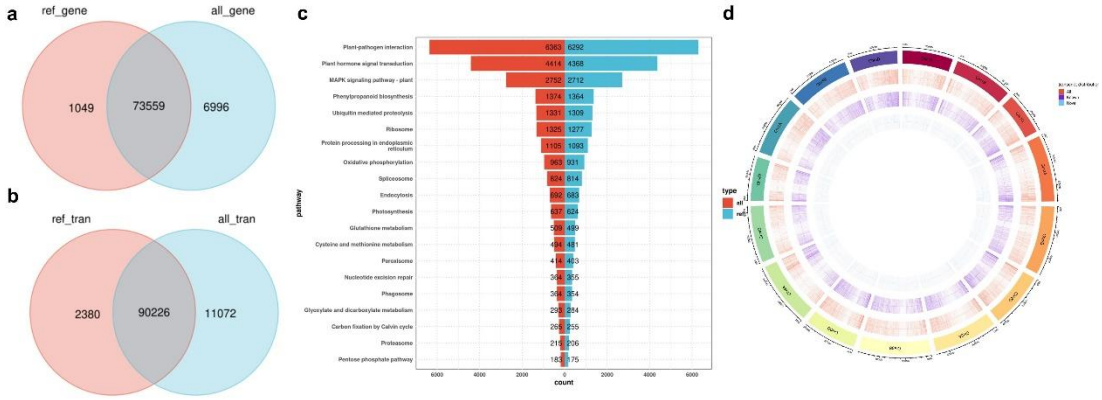


Fig. 2 Comparison of Identification Results: All Transcripts vs. Reference. (a,b) Venn of genes/transcripts: ref vs. all. (c) Differences of pathway annotation: ref vs. all. (d) Density distribution map of the transcriptome. Note: Outermost to innermost-chromosome, all transcripts, known transcripts, novel transcripts-strand-specific.

3.3 Overview of differentially expressed genes of different tissues of wheat

We also analyzed the expression of genes in resistant and susceptible plants in

different tissues using an RNA-sequencing approach. Although biological replicates were collected from different individual plants, tissue samples of the same type exhibited high correlation with each other (Fig. 3a, b). The high correlation based on Pearson's coefficient and clustering of the biological replicates in resistant and susceptible plants indicated that the transcriptome data were reliable. RNA-seq data analysis identified 5764, 5001, and 2286 significantly upregulated genes and 4099, 2250, and 1006 considerably downregulated genes in RL VS. SL (resistant leaf VS. susceptible leaf), RG VS.SG (resistant glume VS. susceptible glume), and RS VS. SS (resistant sheath VS. susceptible sheath) comparison groups, respectively (Fig. 3c). Only 1922 common DEGs were identified at all three tissue points (Fig. 3d). To identify genes exhibiting consistent or tissue-specific transcriptional responses across different tissues, we constructed Venn diagrams of the DEGs from leaf, leaf sheath, and glume tissues. The diagrams revealed that a subset of genes was consistently up- or down-regulated across all three tissues, whereas a large proportion of DEGs displayed tissue-specific expression patterns.

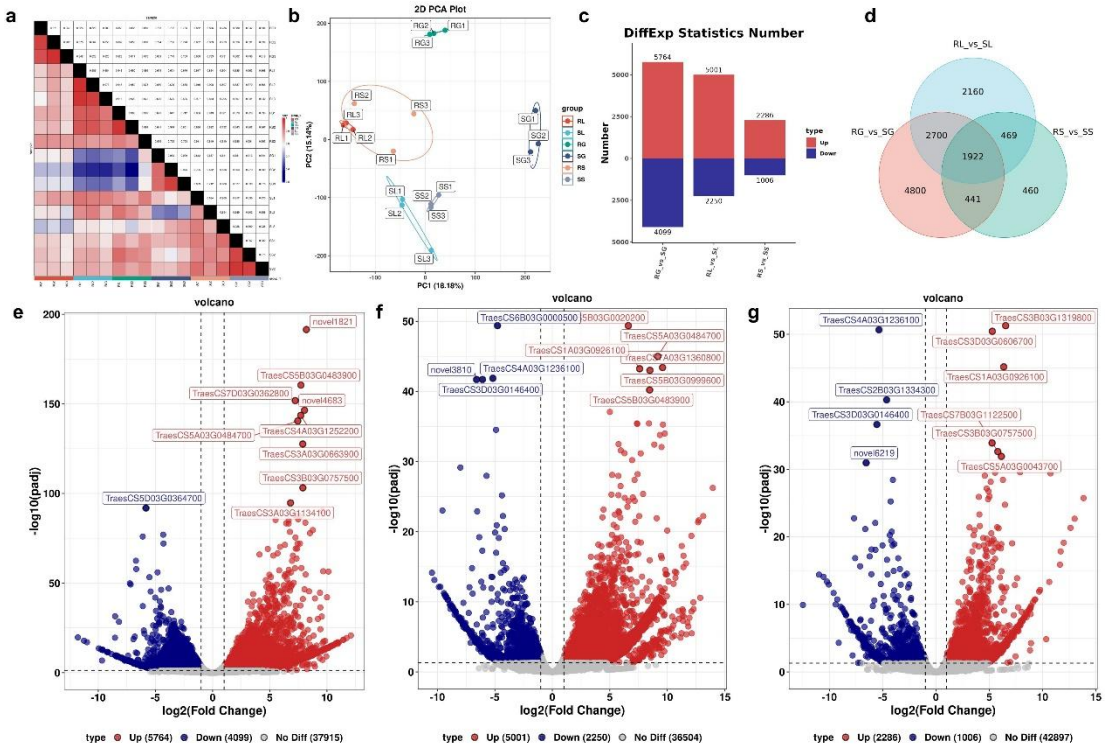


Fig. 3 RNA-seq performed on resistant and susceptible plants at different developmental stages. (a) Sample correlation of all samples. (b) PCA among groups. (c) Differential genes between the various comparison groups. Red means upregulation, and blue means downregulation. (d) Venn diagram of the DEGs. These genes were obtained from RL VS. SL, RG VS. SG, and RS VS. SS comparisons. Volcano plots of differentially expressed genes with up- or down-regulated DEGs in different tissues: sheath(e), leaf(f), and glume (g).

Notably, in all examined tissues, the number of up-regulated genes in ZS57 consistently exceeded that of down-regulated genes relative to ZS54, indicating that pathogen infection predominantly triggers a broad transcriptional activation rather than uniform repression (Fig. S1a-c). This pattern is consistent with the rapid mobilization of defense- and detoxification-related transcriptional programs during pathogen infection [27].

3.4 Transcriptional reprogramming of core metabolic and signaling pathways shared across leaf, sheath, and glume tissue

To identify the systemic molecular programs underlying resistance independently of organ identity, we analyzed the DEGs shared among all three aerial tissues (Fig. 4). Among the coordinately up-regulated genes in the resistant background, the enriched terms converged almost exclusively on chloroplast function and photosynthesis (Fig. 4a): KEGG pathways related to light capture and energy conversion (Photosynthesis-antenna proteins) were uniformly induced, GO cellular component terms were concentrated on the photosystem I/II, thylakoid membrane, and photosystem II oxygen-evolving complex, and the associated molecular functions, including chlorophyll binding and ADP binding, were markedly elevated (Fig. 4a). Concurrently, a distinct cluster of defense-related processes-including innate immune response, immune response, and positive regulation of immune response was also coordinately up-regulated across the three organs, indicating a systemic enhancement of defense recognition in the resistant background. Pathway mapping confirmed sustained expression of core carbon-assimilation enzymes, including ribulose-1,5-bisphosphate carboxylase/oxygenase large subunit (RbcL) and fructose-bisphosphate aldolase (FBA), whereas the anaplerotic enzymes NADP-malic enzyme (NADP-ME) and glutamate-oxaloacetate transaminase (GOT1) showed lower induction relative to the susceptible genotype (Fig. 5d). Gene set enrichment analysis (GSEA) of the leaf comparison, with the resistant genotype ZS54 as the reference, independently confirmed this genome-wide polarization. Photosynthesis-antenna protein-associated gene sets showed

329 significant negative enrichment (downward enrichment curves), indicating their higher
330 expression in the resistant genotype, whereas secondary-metabolism gene sets
331 exhibited the opposite trend (Fig. 4e, f).

332 In sharp contrast, the genes coordinately up-regulated in the susceptible genotype
333 ZS57 relative to the resistant genotype ZS54 across all three tissues defined a conserved
334 susceptibility signature centered on defense signaling and stress metabolism (Fig. 4b).
335 KEGG analysis revealed universal induction of the Mitogen-activated protein kinase
336 (MAPK) signaling pathway-plant, plant-pathogen interaction, amino sugar and
337 nucleotide sugar metabolism, and glutathione metabolism (Fig. 4b). The enriched
338 biological processes were dominated by fungal defense and pathogen recognition
339 (defense response to fungus), cell wall modification and carbohydrate catabolism
340 (chitin metabolic/catabolic process), oxidative stress responses (response to oxidative
341 stress), and secondary metabolism (phenylpropanoid and lignin metabolic process),
342 together with regulatory processes such as protein phosphorylation and jasmonic acid-
343 mediated signaling (Fig. 4b). Pathway mapping localized this activation to the core
344 immune signaling cascades, including the MEKK1-MKK4/5-MPK3/6 module, the
345 CDPK-Rboh respiratory burst branch, and their downstream hypersensitive
346 response(HR)/ Reactive oxygen species (ROS) execution components (Fig. 4c). In the
347 plant-pathogen interaction pathway, CDPK, RIN4 and RPS2 were likewise up-
348 regulated in ZS57 (Fig. S4). Similarly, within the peroxisome pathway, PHYH, FAR
349 and IDH showed consistent induction across all three tissues in the susceptible
350 background.

Taken together, relative to the resistant genotype, susceptible plants display a coordinated shutdown of photosynthetic carbon assimilation and chloroplast function, coupled with a paradoxical hyper-induction of canonical defense signaling cascades-including MAPK pathways, plant-pathogen interaction components, and downstream HR/ROS execution modules. For a hemibiotrophic fungus that transitions from biotrophy to necrotrophy, such unproductive defense hyperactivation and associated cell death are readily exploited to accelerate host tissue necrosis and facilitate colonization. This dual signature of photosynthetic collapse and failed defense regulation provides the transcriptomic basis for the organ-specific disease phenotypes described above and for the cross-genotype comparisons below.

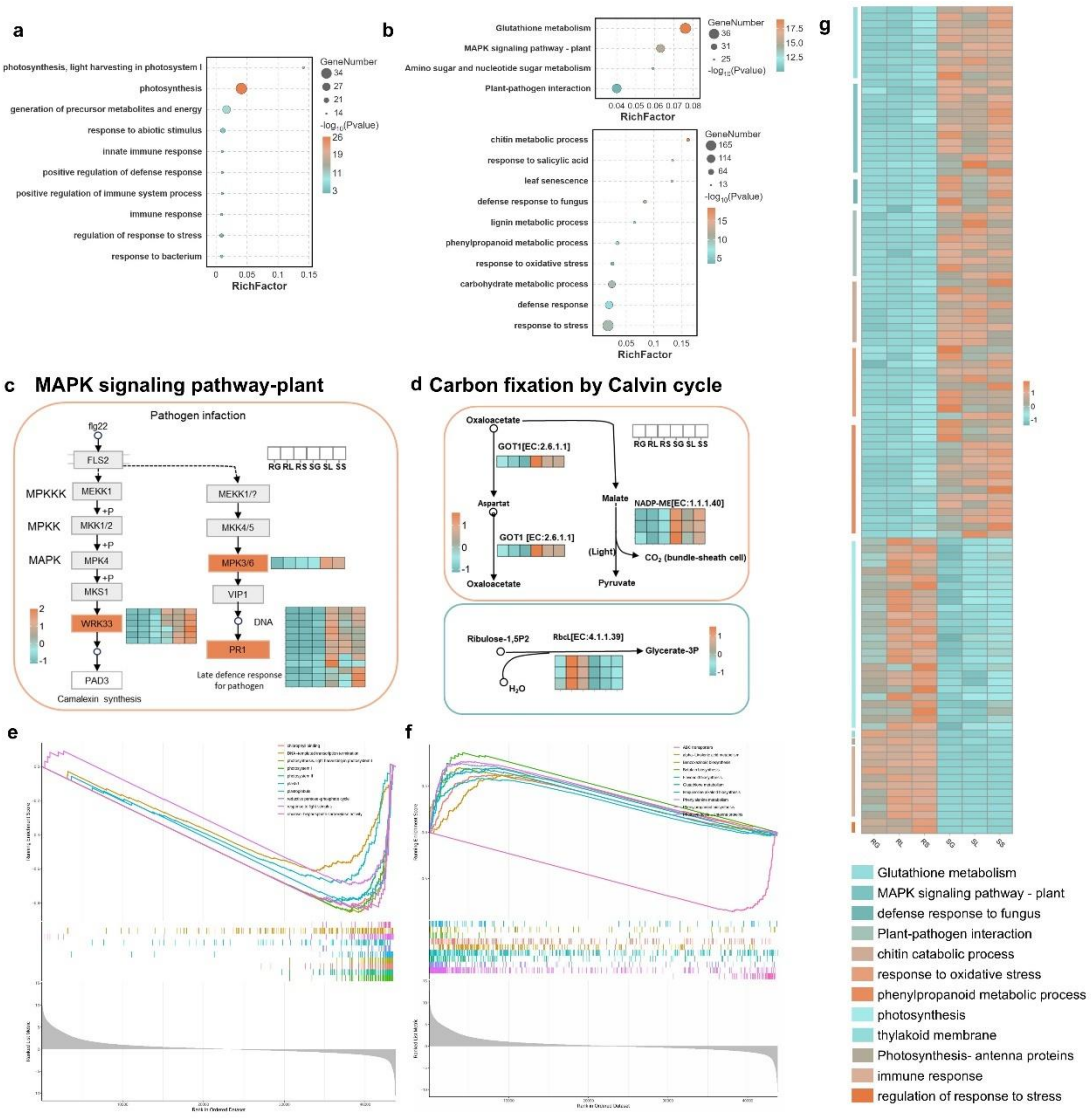


Fig. 4 Functional enrichment and expression profiling of shared DEGs in wheat tissues following *B. sorokiniana* infection. (a) GO and KEGG enrichment bubble plots for shared up-regulated DEGs in ZS54. (b) GO and KEGG enrichment bubble plots for shared up-regulated DEGs in ZS57. Dot size indicates gene count; color gradient represents -log10(P-value). (c, d) Transcriptional profiles and pathway mapping for the MAPK signaling pathway (ko04016) and Calvin cycle (ko00710). Orange and blue denote up- and down-regulation in the susceptible genotype, respectively. (e, f) GO (e) and KEGG (f) Gene set enrichment analysis (GSEA) of leaf transcriptomes with the resistant genotype ZS54 as the reference. (g) Hierarchical clustering heatmaps of representative up- and

down-regulated genes across biological replicates (RG, RL, RS, SL, SG and SS).

3.5 Tissue-specific transcriptional landscapes across leaf, sheath, and glume tissues

To characterize the organ-specific transcriptional responses of wheat to *B. sorokiniana* infection, GO and KEGG enrichment analyses were performed on the DEGs identified in the leaf (RL VS. SL), glume (RG VS. SG), and leaf sheath (RS VS. SS) comparisons of the resistant (R, ZS54) and susceptible (S, ZS57) parents. To reduce redundancy among the enriched terms, semantically similar GO terms were collapsed, and representative terms for each tissue are presented as enrichment bubbles (Fig. 5c-g); the complete enrichment results are provided in Supplementary Table S3.

A strikingly different pattern was observed among the genes up-regulated in the resistant genotype relative to the susceptible genotype (Fig. 5a, c-d). The leaf and glume comparisons shared nearly all enriched terms, whereas the sheath contained 58 uniquely enriched terms and no term was unique to either green organ (Fig. 5a). Genes coordinately elevated in leaves and glumes of the resistant plants were overwhelmingly concentrated on the photosynthetic machinery, including the dark reactions, carbon fixation, photosystem I/II and antenna proteins, chlorophyll metabolism, and chloroplast thylakoid components, together with plant-type cell wall biogenesis, indicating sustained photosynthetic capacity in the two green organs (Fig. 5c). In contrast, genes uniquely up-regulated in the sheaths of the resistant genotype were enriched in immune-related processes, such as innate immune response, defense response to bacterium, and positive regulation of immune response-as well as

391 carbohydrate transport (Fig. 5d), suggesting enhanced defense recognition in this organ.
392 Collectively, these results reveal that resistance to spot blotch is associated with
393 contrasting, organ-specific programs: a conserved maintenance of photosynthetic
394 function shared by the green aerial organs, and a tissue-partitioned defense response in
395 which sheaths emphasize immune recognition and membrane integrity, while leaves
396 and glumes preserve carbon assimilation and structural capacity.

397 Among the up-regulated genes in ZS57, the three aerial organs exhibited clearly
398 distinct functional profiles (Fig. 5b, e-g). The glume comparison contained the largest
399 number of tissue-specific enriched terms (138), followed by the leaf (51) and the leaf
400 sheath (15) (Fig. 5b). Genes uniquely up-regulated in the infected sheaths were
401 predominantly associated with extracellular defense and redox homeostasis, including
402 peptidase/serine-type endopeptidase inhibitor activities, peroxidase and antioxidant
403 activities, and sphingolipid metabolism (Fig. 5g), suggesting an active reinforcement
404 of cell walls coupled with localized oxidative responses in this organ. In the leaves,
405 uniquely enriched terms converged on primary carbon remodeling and membrane lipid
406 turnover, including galactose and hexose metabolism, fatty acid β-oxidation, and
407 linoleic acid metabolism, together with hormone-responsive and lignin biosynthetic
408 processes, reflecting the mobilization of carbon reserves and accelerated membrane
409 disassembly characteristic of senescing source tissue (Fig. 5e). In the glumes, up-
410 regulated genes were enriched in central energy metabolism (glycolysis, TCA cycle,
411 aerobic respiration), nitrogen assimilation (arginine biosynthesis and metabolism), and
412 specialized secondary metabolism (sesquiterpene, flavonoid, and stilbenoid

biosynthesis), as well as jasmonic acid-related stress signaling, consistent with a sink-to-defense metabolic transition in infected floral tissues (Fig. 5f).

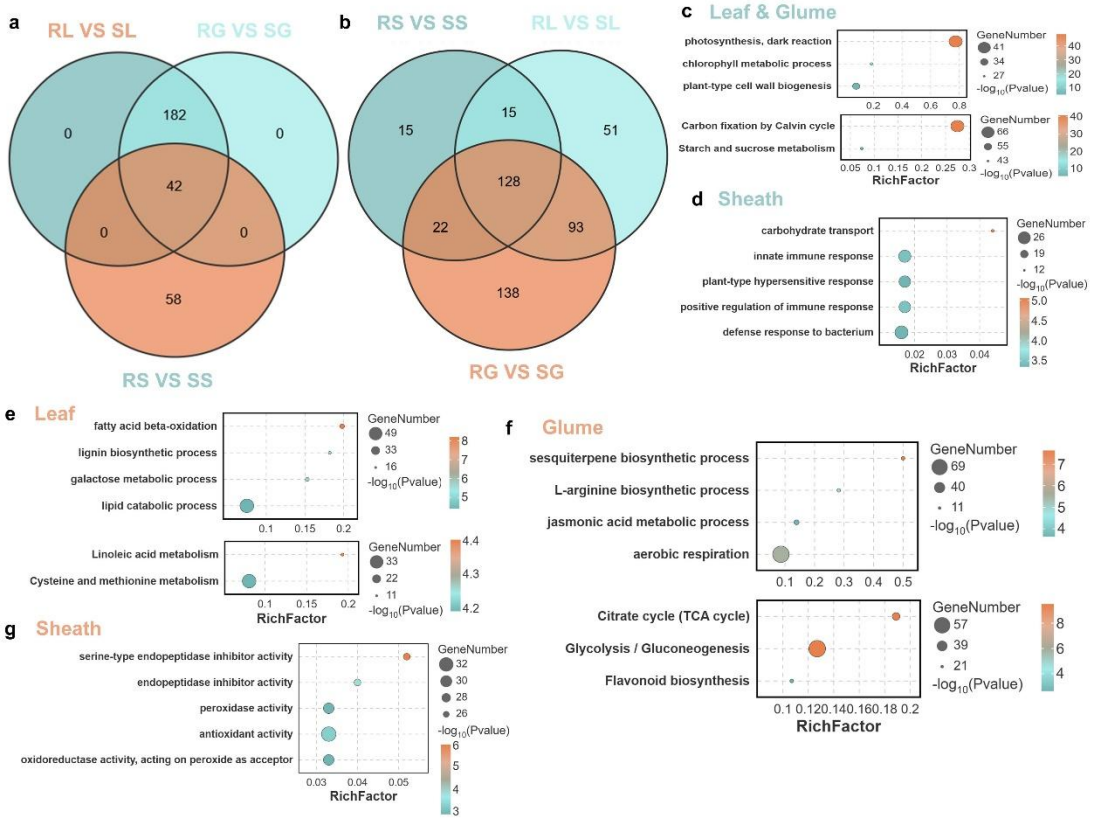


Fig. 5 Comprehensive transcriptional dynamics and functional enrichment analyses of up- and down-regulated DEGs across aerial organs of susceptible versus resistant wheat. (a, b) Venn diagrams showing overlap of enriched GO and KEGG terms among leaf, glume, and leaf sheath comparisons for genes up-regulated in ZS54 (a) and ZS57 (b). (c-g) Bubble plots of enriched GO categories and KEGG pathways. Shared terms in leaf and glume of ZS54 (c); unique terms in the sheath of ZS54 (d); tissue-specific terms in ZS57 leaf (e), glume (f) and sheath (g). Dot size represents the number of genes enriched in each term, and the color gradient corresponds to the -$\log_{10}$ (P-value).

3.6 Co-expression network analysis identifies susceptibility-associated modules and hub genes

To further analyze the expression characteristics of DEGs and identify gene modules and co-expressed genes associated with disease susceptibility, WGCNA was

performed on DEGs identified from the transcriptome data. As the input trait data, disease susceptibility was recorded as a binary phenotype for each sample, with resistant and susceptible materials assigned values of 0 and 1, respectively, for the leaf sheath, leaf, and glume, respectively. A weighted co-expression network was constructed using the dynamic tree- cutting method, yielding 67 expression modules (Fig. 6 a).

These modules were correlated with disease susceptibility traits in leaf sheaths, leaves, and glumes, respectively. The darkorange module showed a strong association with disease susceptibility in leaf sheaths (correlation coefficient=0.94), the red module with disease susceptibility in leaves (correlation coefficient = 0. 76), and the turquoise module with disease susceptibility in glumes (correlation coefficient = 0. 89) (Fig. 6b). The darkorange module contained 447 genes, the turquoise module contained 7,382 genes, and the red module contained 2,537 genes. The clustering diagram and the clustering heatmap of the correlation between phenotype and module are shown in Fig. S5. Subsequent analyses were conducted on these modules.

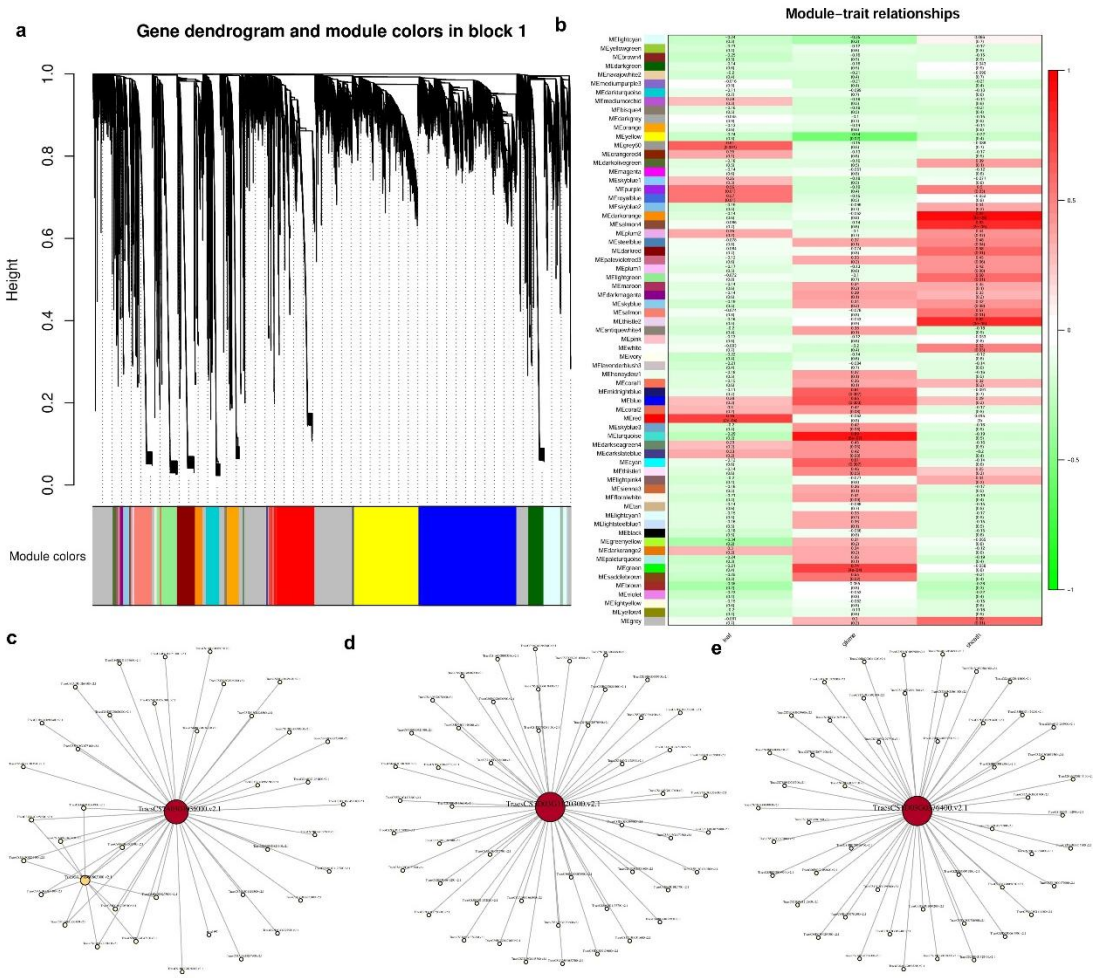
To validate the relationships of the darkorange, turquoise, and red modules with disease susceptibility, scatter plots of module eigengene expression versus disease susceptibility phenotypes were generated. The darkorange module was significantly correlated with leaf sheath disease susceptibility ($r=0.86$, $P< 4.2e-132$) (Fig. S5a), the turquoise module with glume disease susceptibility ($r=0.78$, $P< 1e-200$) (Fig. S5b), and the red module with leaf disease susceptibility ($r=0.42$, $P< 5.6e-109$) (Fig. S5c).

Gene weight relationships within these modules were calculated and visualized

using Cytoscape software (Fig. 6c-e). Hub genes identified in the modules were as follows: *TraesCS7A03G1036000* and *TraesCS1D03G0863000* in the darkorange module (Fig. 6c); *TraesCS3D03G1120300* in the turquoise module(Fig. 6d); and *TraesCS1D03G0376400* in the red module(Fig. 6e).

Functional annotation indicated that *TraesCS7A03G1036000* encodes a probable xyloglucan endotransglucosylase/hydrolase protein 23, which is involved in cell wall biosynthesis and the metabolic process of xyloglucan. *TraesCS3D03G1120300* encodes a pentatricopeptide repeat- containing protein that promotes RNA binding, protein binding, and zinc ion binding, and participates in RNA modification. *TraesCS1D03G0376400* encodes a PPPDE thiol peptidase family protein (putative) that promotes peptidase activity and is involved in protein modification by removal of small protein modifiers (Table S4).

Taken together, the WGCNA revealed that disease susceptibility in the three tissues is governed by largely distinct co-expression modules, with the darkorange, red, and turquoise modules capturing the tissue-specific transcriptional programs of the leaf sheath, leaf, and glume, respectively. The hub genes identified in these modules encode proteins implicated in cell wall remodeling, RNA modification, and protein processing, suggesting that cell wall reinforcement together with post-transcriptional and post-translational regulation may collectively contribute to the differential spot blotch susceptibility observed among wheat materials.



469

470 **Fig. 6 WGCNA for hub gene identification.** (a) Module clustering diagram; (b) Statistical results of the

471 correlation between the module and the phenotype; (c-e) Network diagram of genes within the darkorange (c),

472 turquoise (d), and red (e) module.

473 **3.7 Analysis of alternative splicing events**

474 As mentioned above, we identified 11,072 novel isoforms in our transcriptome

475 (Fig. 2b, d). A considerable proportion of novel transcripts in the transcriptome may

476 originate from alternative splicing (AS) as well as from extensions or truncations at the

477 5′ or 3′ ends of mRNA. Following transcription, a long chain of adenine nucleotides,

478 known as the poly(A) tail, is appended to the 3′ end of mRNA molecules and plays an

479 essential role in maintaining transcript stability and regulating translation [28]. When

multiple poly(A) signals are present within the same transcript, alternative polyadenylation (APA) can occur, giving rise to transcripts with distinct 3′ ends and thereby enriching transcriptome diversity [29]. To characterize the distribution of polyadenylation sites, the identified Poly(A) sites (PACs) were annotated against genomic regions (Fig. 7a). The results showed that more than 90% of the PACs (91.31%) were mapped to the 3′UTR, whereas the remaining regions contained only minor fractions, with the intron, CDS, and exon accounting for 3.42%, 2.61%, and 2.30%, respectively, and the 5′UTR showing the lowest proportion (0.35%). This pronounced enrichment of poly(A) sites at the 3′ end of transcripts agrees well with the molecular mechanism of mRNA polyadenylation, corroborating the accuracy of PAC identification and providing a solid basis for the subsequent APA analyses.

In addition, the number of PACs per gene was statistically analyzed (Fig. 7b). It was found that 45.97% of genes contained a single poly(A) site, while 30.79% and 15.16% of genes harbored two and three sites, respectively, and approximately 8.07% of genes contained four or more sites, indicating that the majority of genes possessed the structural basis for APA. Moreover, analysis of the usage preference of the major proximal and distal poly(A) sites showed that, taking the glume tissue as an example, 7,621 genes exhibited preferential usage of distal poly(A) sites whereas 3,983 genes favored proximal sites in ZS57 compared with ZS54 under disease conditions, with a ratio of approximately 1.9:1; this ratio was 1.82:1 in the leaf and 1.63:1 in the leaf sheath (Fig. 7c; Fig. S6). This result indicated that more genes tended to utilize distal poly(A) sites, generating transcripts with extended 3′UTRs in all three tissues under

disease conditions, which may alter transcript stability and translation efficiency by incorporating additional miRNA and RNA-binding protein regulatory elements.

AS is an important post-transcriptional process of gene expression that affects the stability of transcripts and increases the diversity of proteins. A total of 16,845 (60.7%) genes were found to possess two or more alternative splicing variants in this transcriptome (Fig. 7d). Moreover, seven major types of AS events were discovered in the samples, including exon skipping (SE), intron retention (RI), alternative last exon (AL), alternative first exon (AF), mutually exclusive exon (MX), alternative 5′ splice sites (A5), and alternative 3′ splice sites (A3). A3 was the most abundant type of AS events, accounting for more than 39% of all AS events in both ZS57 and ZS54 (Fig. 7e; Table S5). In both cultivars, the proportion of AF events was higher in ZS57 than in ZS54, which might be associated with disease susceptibility, whereas the proportions of the remaining types of AS events showed no obvious difference between the two cultivars. Together, these results reveal extensive post-transcriptional remodeling-both at the level of poly(A) site choice and splicing-in the wheat response to *B. sorokiniana*, and provide a resource of alternative isoforms for identifying candidate resistance or susceptibility determinants.

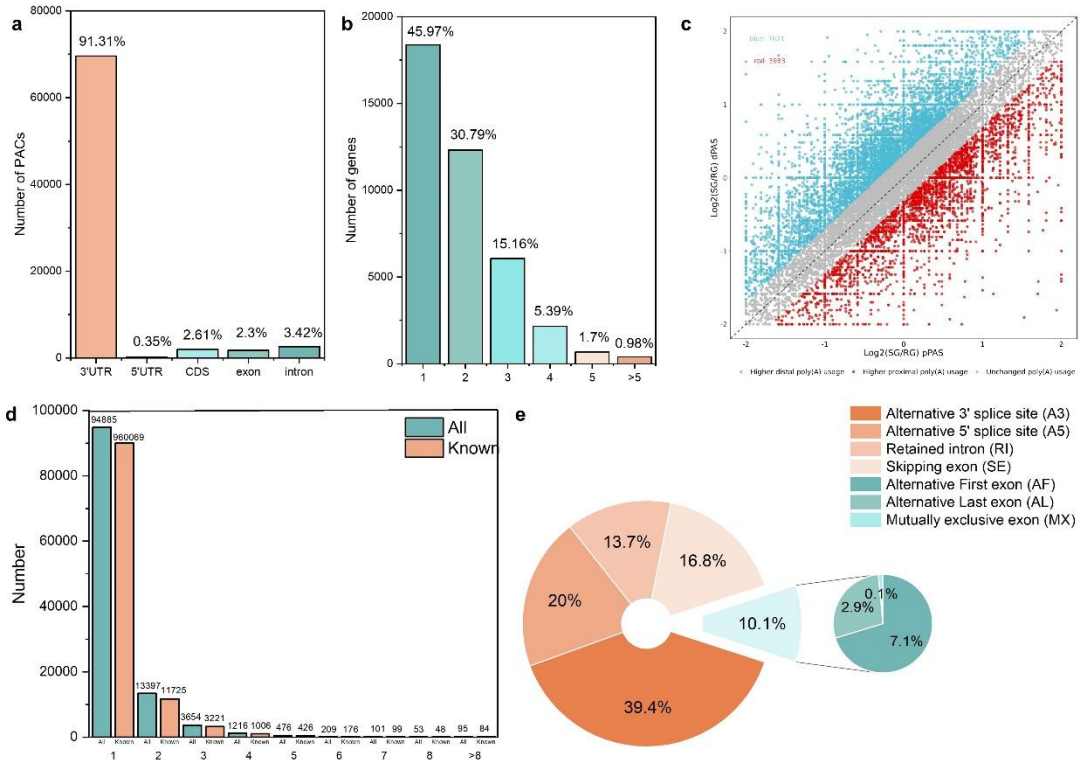


Fig. 7 Analysis of alternative polyadenylation and alternative splicing events. (a) The distribution map of PACs in various regions of the gene; (b) PAC quantity distribution chart; (c) Preference for poly(A) sites of RG VS. SG; (d) The number of genes with different numbers of transcripts; (e) Variable splicing type and special statistical chart.

3.8 Intersectional functional enrichment uncovers shared resistance-associated and susceptibility-associated transcriptional programs

To test whether the resistance-associated transcriptional signature described above is conserved across genetic backgrounds, we integrated an independent full-length leaf transcriptome dataset from the resistant-susceptible pair ZS31(R)/ZS3(S), whose resistance locus is located on a different chromosome from that of ZS54(R)/ZS57(S) (sequencing statistics are provided in Supplementary Table S2 and Fig. S2 and Fig. S3). To uncover the structural and functional basis of the sustained photosynthetic competence shared across resistant wheat genotypes, an intersectional functional

enrichment analysis was performed on genes responsive to *B. sorokiniana* infection in the resistant lines ZS54(R) and ZS31(R) relative to their respective susceptible controls (Fig. 8a); the complete enrichment results of ZS31(R)/ZS3(S) are provided in Supplementary Table S6. A four-way comparison of the enriched GO and KEGG terms identified 54 commonly up-regulated terms and 150 commonly down-regulated terms shared by the two resistant lines. Notably, no terms were found that were down-regulated in ZS54(R) but up-regulated in ZS31(R), whereas only four divergent terms showed the opposite pattern, being up-regulated in ZS54(R) yet down-regulated in ZS31(R) (Fig. 8a)-i.e., down-regulated in ZS57(S) yet up-regulated in ZS3(S).

Conserved Photosynthetic Activation Across Resistant Genotypes

Both GO and KEGG evaluations revealed a profound, synchronized enrichment of chloroplast and photosynthesis-related terms among the commonly up-regulated groups in ZS54 and ZS31 (Fig. 8b, c). In terms of cellular components, terms strictly localized to the chloroplast, plastid, thylakoid, and chloroplast thylakoid membrane were prominently enriched (Fig. 8b). Consistently, pathway analysis highlighted that core KEGG networks-specifically Photosynthesis, Photosynthesis- antenna proteins, Carbon fixation in photosynthetic organisms, and Porphyrin and chlorophyll metabolism-underwent marked transcriptional activation (Fig. 8c). Notably, genes responsive to abiotic stimuli, radiation, and light were also coordinately enriched, indicating concurrent activation of general stress-response programs. Together, these results indicate that during fungal infection, both ZS54 and ZS31-despite carrying different disease-resistance loci-exhibit coordinated transcriptional enhancement of

chloroplast structure, photosynthetic machinery, and associated stress-responsive processes. This reinforcement may contribute to the maintenance of photosynthetic function and enhanced stress tolerance in the resistant materials.

Conserved Transcriptional Up-Regulation of Defense, Secondary Metabolism, and Stress Responses Across Susceptible Genotypes

To identify core transcriptional responses associated with susceptibility independently of genetic background, analysis of the 150 shared up-regulated terms in ZS57 yet up-regulated in ZS3 was conducted (Fig. 8d-h). KEGG pathway analysis revealed significant enrichment in pathways related to secondary metabolism and stress detoxification, specifically Phenylpropanoid biosynthesis, Phenylalanine metabolism, Biosynthesis of secondary metabolites, Glutathione metabolism, Amino sugar and nucleotide sugar metabolism, and alpha-Linolenic acid metabolism (Fig. 8d).

In terms of BP, commonly enriched terms converged heavily on defense, including defense response, response to fungus, response to biotic stimulus, and response to external biotic stimulus (Fig. 8f). Concurrently, pathways governing oxidative stress defense and structural modification-such as response to oxidative stress, response to oxygen-containing compound, detoxification, response to toxic substance, cell wall macromolecule metabolic/catabolic processes, and chitin metabolic process-showed widespread induction (Fig. 8e, h). Furthermore, hormone-signaling and development-associated processes, including jasmonic acid biosynthetic process, oxylipin metabolic/biosynthetic process, response to salicylic acid, and leaf senescence, were prominently represented among the shared up-regulated genes (Fig. 8 g).

Divergent Transcriptional Regulation of Secondary Metabolism and Structural Integrity

To uncover genetic background-dependent variations underlying susceptibility, intersectional analysis focused on the 4 divergent terms found down-regulated in ZS57(S) (equivalent to up-regulated in its resistant counterpart ZS54) but up-regulated in ZS3(S) (Fig. 8a). This subset revealed striking divergence in secondary metabolism, lipid dynamics, and structural maintenance. Notably, genes associated with Flavonoid biosynthesis and lyase activity were distinctly upregulated in ZS3 while being suppressed in ZS57. Furthermore, biological processes governing fatty acid metabolic process and cellular anatomical structure exhibited opposing regulatory patterns between the two susceptible lines. While ZS57 displayed a wholesale shutdown of membrane lipid and structural preservation pathways, ZS3 retained an active, albeit partial, transcriptional engagement in flavonoid-mediated chemical defense and lipid remodeling, highlighting distinct pathoadaptive strategies within similar phenotypic susceptibility categories.

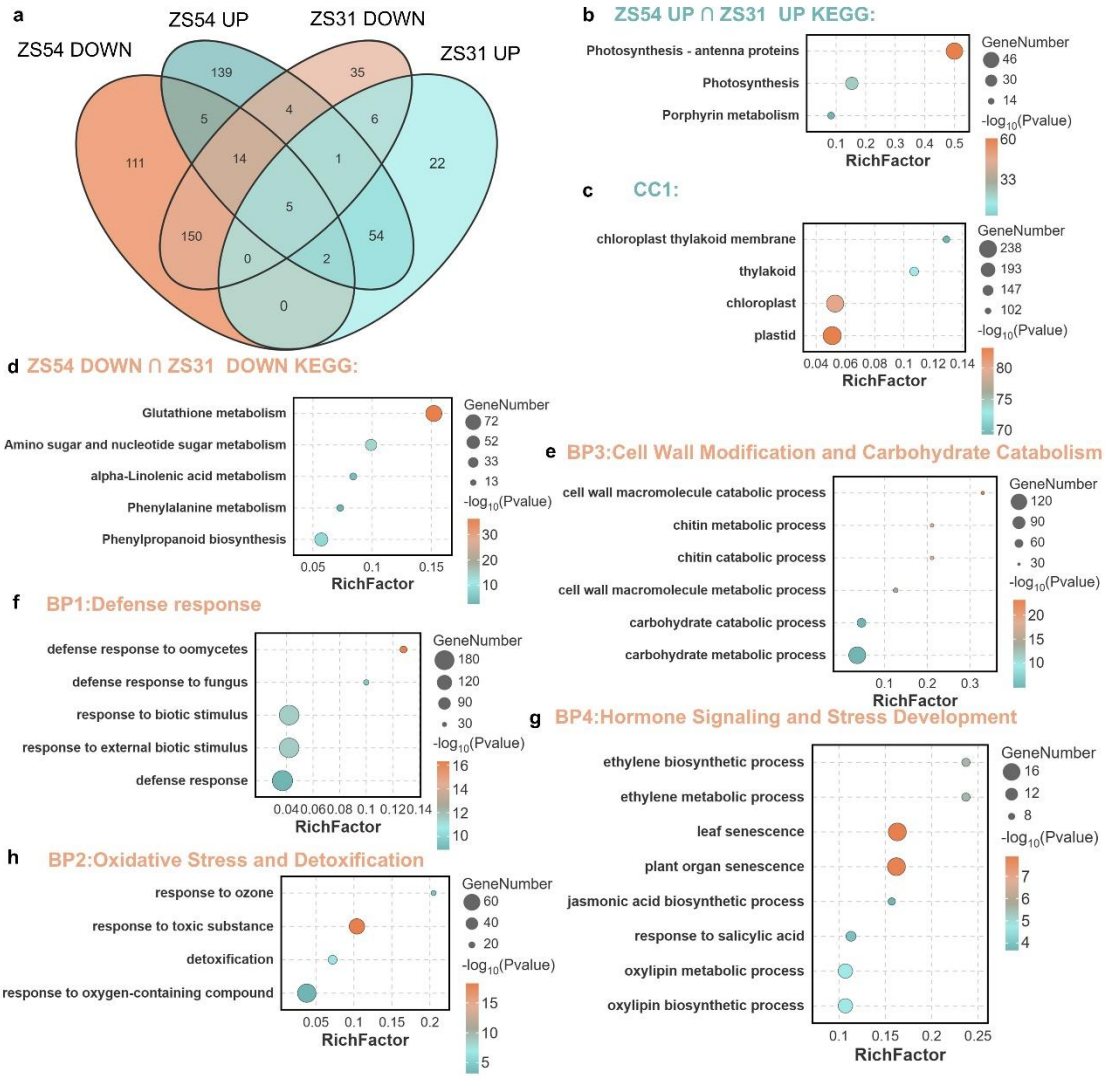


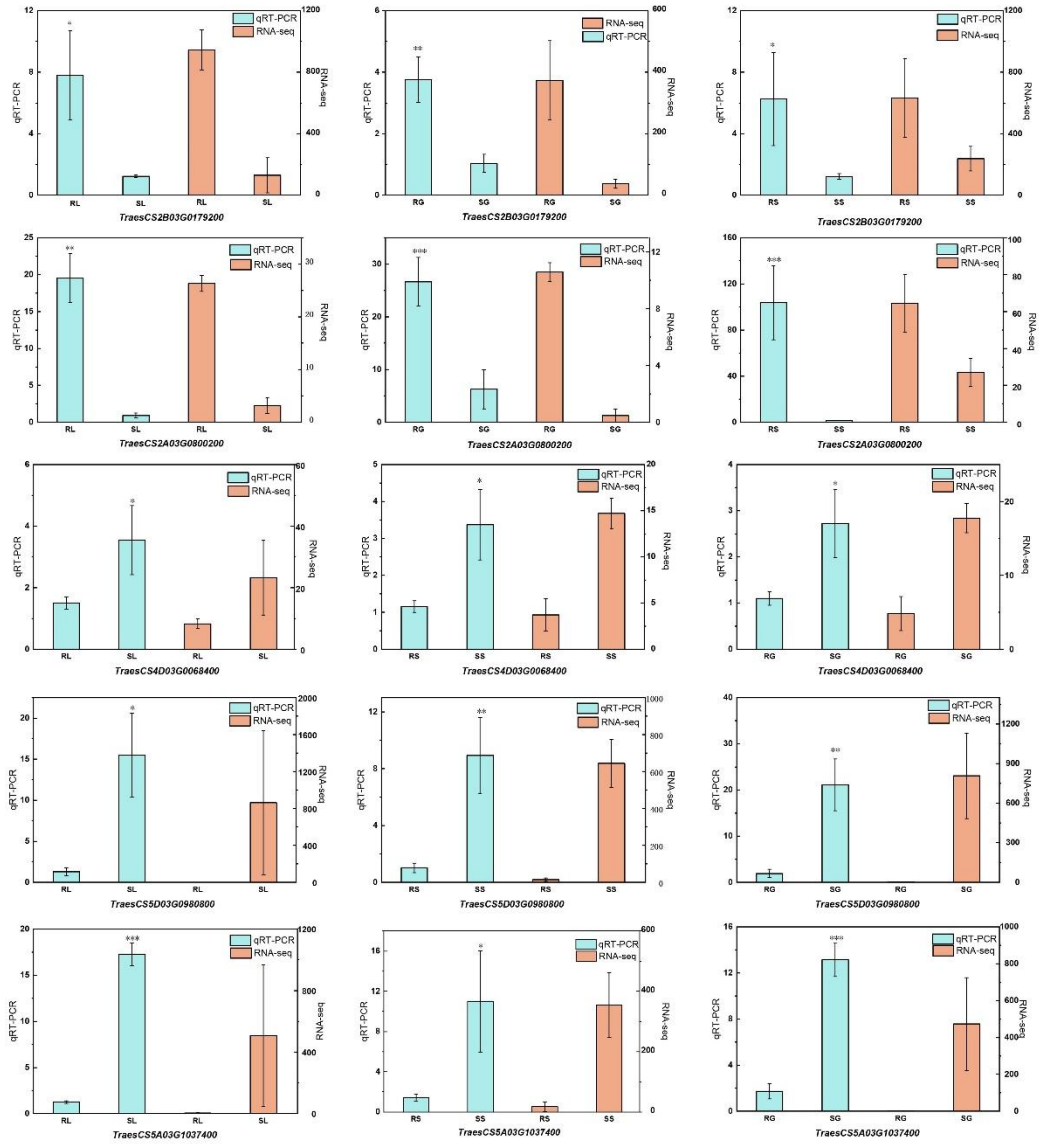
Fig. 8 Intersectional and functional enrichment analyses of transcriptional responses in resistant wheat lines (ZS54 and ZS31) relative to their susceptible controls. (a) Venn diagram illustrating the overlap of enriched GO and KEGG terms between the ZS54 and ZS31 comparisons, highlighting shared and divergent regulatory patterns. (b-c) Common up-regulated enrichment terms. (d-h) Common down-regulated enrichment terms.

3.9 Validation of the expression levels of several key genes

Building on the pathway-level findings described above, in which MAPK signaling, plant-pathogen interaction, photosynthesis, the Calvin cycle, and peroxisome metabolism were identified as central to the divergent resistant and susceptible responses, we next sought to validate these transcriptome-derived expression patterns

602 at the single-gene level.

603 To validate the observed expression changes of defense-related genes, qRT-PCR
604 was performed on independent biological samples. We selected genes involved in
605 photosynthesis (*TraesCS2A03G0800200*), one gene associated with the Calvin cycle
606 (Rbcl, *TraesCS2B03G0179200*), two genes from MAPK singnaling pathways (PR1,
607 *TraesCS5D03G0980800* and *TraesCS5A03G1037400*), and one gene related to the
608 peroxisome pathway (PHYH, *TraesCS4D03G0068400*) to corroborate the RNA-seq
609 data. The qRT-PCR results were largely consistent with the RNA-seq data, thereby
610 validating the reliability of the transcriptomic analysis (Fig. 9). All primer sequences are
611 provided in Table S7.



612

613 **Fig. 9 qRT-PCR validation of differentially expressed genes in different tissues of ZS54 and ZS57.** The

614 relative transcript levels among different samples were quantified by the $2^{-\Delta\Delta Ct}$ method, with *Triticum aestivum L.*

615 EF1A1 gene as the reference gene for normalization.

616 **4. Discussion**

617 Spot blotch, caused by the hemibiotrophic fungus *B. sorokiniana*, remains a major

618 constraint on wheat production in warm and humid regions, where yield losses can

619 reach 40-44% in susceptible cultivars[30]. Although several major resistance genes

(*Sb1-Sb4* and *SbWE35*) and QTLs have been mapped, the transcriptional programs that render certain genotypes highly susceptible-particularly their organ specificity and post-transcriptional complexity-are still incompletely understood. Therefore, it is essential to understand the susceptibility mechanism of wheat to spot blotch infection for developing new strategies to promote wheat disease resistance breeding.

Conserved photosynthetic module and residual metabolism tune disease severity across different resistance loci

Despite their resistance loci being located on different chromosomes, cross-genotype comparison of the two pairs (ZS54/ZS57 and ZS31/ZS3) revealed a highly conserved transcriptional programme. Among the 54 shared up-regulated terms, the dominant categories were chloroplast organisation and photosynthetic function, including plastid and thylakoid components, photosystems I and II, light harvesting, carbon fixation, chlorophyll binding, and porphyrin/chlorophyll metabolism. Both resistant genotypes also coordinately activated terms related to abiotic stimuli, radiation, and light. Thus, although the two resistant lines carry different resistance alleles, they converge on a similar downstream module that couples photosynthetic maintenance with general stress acclimation.

This convergence is biologically plausible because sustained photosynthetic capacity is essential for maintaining energy supply, redox homeostasis, and overall tissue integrity under biotic stress. In the present study, both resistant genotypes (ZS54 and ZS31) exhibited coordinated up-regulation of chloroplast organisation, light-harvesting, and carbon-fixation pathways and remained free of visible lesions

642 throughout the season. In contrast, the susceptible genotypes displayed systemic down-
643 regulation of the same pathways accompanied by rapid lesion expansion and tissue
644 necrosis. Chloroplasts are not only sites of energy production but also platforms for
645 ROS generation, Ca^{2+} signalling and retrograde regulation of nuclear genes [31–33].
646 Pathogen effectors frequently target chloroplasts to disrupt photosynthetic electron
647 transport and suppress chloroplast-derived ROS bursts, thereby facilitating infection
648 [34]. The transcriptional reinforcement of photosynthetic machinery observed
649 exclusively in the resistant lines may therefore help preserve ATP/NADPH supply, limit
650 uncontrolled ROS accumulation and support continued cellular function, thereby
651 preventing the transition to irreversible tissue collapse. These co-enriched pathways
652 should be interpreted as a protective acclimation response that contributes to the
653 absence of disease symptoms rather than as direct evidence of causal resistance.

654 Despite this shared susceptible signature, a few divergent terms distinguished the
655 two disease-severity trajectories. ZS3 retained activation of flavonoid biosynthesis,
656 lyase activity, fatty-acid metabolism, and structural-maintenance processes, whereas
657 these pathways were suppressed in the more severely affected ZS57 (Disease Severity
658 Modulation in Fig. 10). Because flavonoids act both as antimicrobial compounds and
659 as redox buffers [35–39], their residual engagement likely slows, without preventing,
660 disease progression. Collectively, these results support a continuum model of disease
661 severity in which major resistance loci determine the overall resistance state, while
662 retention or loss of secondary-metabolic and structural capacity modulates the rate and
663 extent of symptom development. Such severity modifiers should be considered

alongside major resistance loci in marker-assisted selection.

Systemic conservation of photosynthetic competence and organ-specific metabolic exploitation

The most conserved feature across resistant genotypes and all green aerial organs was the coordinated activation of light reactions, antenna proteins, carbon fixation, and chlorophyll metabolism-an up-regulation of the entire photosynthetic apparatus that contrasts with the resource reallocation away from carbon assimilation typically observed in compatible interactions [40, 41]. In the resistant background, sustained expression of RbcL and fructose-bisphosphate aldolase supports continued Calvin-cycle activity, whereas the anaplerotic enzymes NADP-malic enzyme and glutamate-oxaloacetate transaminase showed higher induction in the susceptible genotype, suggesting a compensatory attempt to sustain organic-acid and NADPH supply when the Calvin cycle fails [42, 43]. The metabolic fate of the mobilized resources was organ-specific (Fig. 10). In infected leaves, the up-regulation of galactose and hexose metabolism, fatty acid β-oxidation, and linoleic acid metabolism signals aggressive carbon export and membrane dismantling in senescing source tissue [44, 45]. In infected glumes, the activation of glycolysis, the TCA cycle, arginine metabolism, and sesquiterpene and flavonoid biosynthesis reflects a sink-to-defense transition that simultaneously sustains residual grain filling and antimicrobial compound production [46–48]. While phenylpropanoid metabolism was systemically induced in susceptible tissues, the additional enrichment of flavonoid and stilbenoid pathways in glumes may contribute to a possible metabolic context for the dark pigmentation frequently

observed on infected spikes [49, 50]. Direct causal links, however, remain to be experimentally verified. Thus, *B. sorokiniana* appears to exploit the pre-existing physiological identities of aerial organs rather than imposing a uniform transcriptional response.

The defense paradox: hyperactivation of HR/ROS programs benefits the necrotroph

A second conserved signature was the systemic induction of MAPK signaling, plant-pathogen interaction, glutathione, and phenylpropanoid pathways (Fig. 10)-transcriptional features that normally denote successful resistance, yet here coincided with severe disease. This paradox is well documented for hemibiotroph-to-necrotrophs, which exploit host hypersensitive-response-like cell death and ROS bursts as substrates for colonization [51–53]. Pathway mapping localized the induction to the MEKK1-MKK4/5-MPK3/6 cascade, the CDPK-Rboh respiratory burst branch, and their downstream HR executioners [54, 55]-programs that effectively restrict biotrophs [56], but are predicted to accelerate necrosis against a necrotroph and hemibiotroph. Prior comparative studies similarly showed that resistant wheat genotypes deploy MAPK and hormone cascades more promptly, whereas susceptible genotypes mount a stronger but mistimed response that correlates with more severe symptoms [18, 57, 58]. Our data therefore caution against interpreting "defense response" enrichment as protective in this pathosystem, and nominate calibration of cell-death circuits-rather than their further activation-as the more rational intervention. The overall transcriptional architecture integrating these conserved and organ-specific programmes is summarized

in Fig. 10.

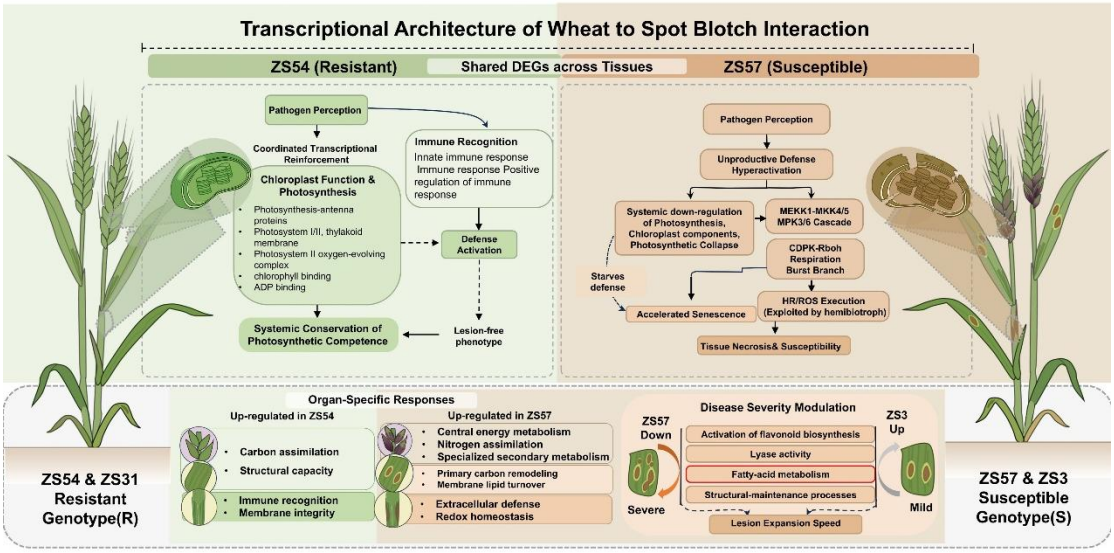


Fig. 10 Conceptual model of the transcriptional architecture underlying wheat responses to spot blotch. The model summarizes the conserved and organ-specific transcriptional programmes identified in this study. In resistant genotype ZS54, pathogen perception triggers coordinated reinforcement of chloroplast function and photosynthesis together with immune recognition, resulting in conserved photosynthetic competence and a lesion-free phenotype. In susceptible ZS57, the same perception leads to unproductive defence hyperactivation (MAPK and CDPK-Rboh pathways) coupled with systemic photosynthetic collapse, accelerating senescence and tissue necrosis that benefits the hemibiotroph. Organ-specific responses further differentiate the interaction: resistant tissues maintain carbon assimilation, structural capacity, and membrane integrity; residual flavonoid and structural capacity in ZS3 moderate lesion expansion relative to the more severe phenotype of ZS57. Susceptibility is thus an active, organ-dependent process modulated by both shared transcriptional signatures and quantitative metabolic differences.

Organ-dependent susceptibility: distinct molecular failures revealed by co-expression networks

WGCNA was performed with susceptibility as the target phenotype, because susceptibility behaves as the dominant trait in the ZS57 × ZS54 hybrid population; accordingly, modules were correlated with the susceptibility score to identify molecular

programs associated with the dominant susceptible phenotype. This analysis assigned a distinct molecular hub to each organ, reinforcing the organ-dependence of susceptibility. In sheaths, the hub gene encoding a xyloglucan endotransglucosylase/hydrolase, together with an ABA-inducible factor, implicates ABA-mediated cell-wall loosening in facilitating pathogen ingress, consistent with the established antagonism of salicylic acid-dependent defense by ABA [59–63]. In glumes, a pentatricopeptide repeat (PPR) protein hub points to chloroplast and mitochondrial RNA-metabolic dysfunction as a driver of floral tissue vulnerability [34, 64]. In leaves, a PPPDE thiol peptidase hub suggests disrupted proteostasis of defense regulators [65–67]. Notably, sheaths uniquely suppressed immune-recognition genes while reinforcing cell walls, potentially creating a transiently permissive niche. Susceptibility thus emerges not as a single program but as a family of organ-specific failures, which implies that durable resistance may need to be assembled organ by organ.

Post-transcriptional remodeling by AS and APA expands the susceptibility repertoire

Beyond gene-level expression, full-length sequencing resolved a substantial post-transcriptional layer. Over 60% of expressed genes produced multiple isoforms, with alternative 3′ splice sites predominant and alternative first exon usage specifically elevated in the susceptible line, implicating transcription start-site choice rather than canonical splicing as a distinguishing feature of the susceptible response [29]. At the 3′ end, infection shifted poly(A) site usage toward distal positions in all three organs, systematically extending 3′UTRs. Because 3′UTR configuration and poly(A) tail

748 dynamics govern mRNA stability, localization, and translational efficiency [28], this
749 shift may stabilize defense- and metabolism-related transcripts during infection,
750 although this awaits direct experimental testing. Together with the 6,996 newly
751 annotated genes that were disproportionately associated with plant-pathogen interaction
752 categories, these alternative isoforms substantially expand the candidate pool of
753 susceptibility determinants and constitute a community resource that would have been
754 inaccessible to short-read sequencing [68].

755 **Implications for breeding durable resistance**

756 The convergence of the systemic signature, the tissue-resolved co-expression
757 networks, and the cross-genotype comparison points to three breeding levers:
758 protecting chloroplast integrity to delay the photosynthetic collapse that starves defense
759 and fuels senescence; calibrating HR/ROS execution nodes (such as MPK3/6 and Rboh)
760 so that induced defenses do not become colonization substrates; and maintaining cell-
761 wall reinforcement and flavonoid capacity, whose residual activity already
762 differentiates severe from mild susceptibility. The hub genes identified here-the XTH,
763 the PPR protein, and the PPPDE thiol peptidase-together with the AF- and APA-
764 associated transcripts, are logical entry points for functional validation.

765 **5. Conclusion**

766 This study demonstrates that susceptibility of wheat to *B. sorokiniana* is an active,
767 organ-dependent process rather than a passive absence of resistance. Multi-tissue
768 Oxford Nanopore full-length transcriptome profiling of the contrasting pair ZS54/ZS57,
769 integrated with an independent leaf dataset from ZS31/ZS3, revealed a conserved dual

signature of susceptibility: systemic collapse of photosynthetic capacity accompanied by unproductive hyperactivation of MAPK signalling, plant-pathogen interaction, and HR/ROS pathways that favour necrotrophic colonization.

Importantly, although the resistance loci in the two genetic backgrounds reside on different chromosomes, the core transcriptional programmes underlying resistance and susceptibility are largely shared. Both resistant genotypes displayed coordinated reinforcement of chloroplast organisation, light-harvesting and carbon-fixation pathways and remained free of visible lesions, consistent with a protective acclimation response that helps maintain energy supply, redox homeostasis and tissue integrity. In contrast, both susceptible genotypes exhibited photosynthetic down-regulation accompanied by rapid lesion expansion. The principal difference between the two susceptible lines lay in residual flavonoid biosynthetic capacity, which appears to modulate quantitative disease severity.

Tissue-resolved analyses further showed that leaves, sheaths and glumes deploy distinct metabolic programmes under infection, while weighted gene co-expression network analysis identified organ-specific modules and hub genes involved in cell-wall remodelling, RNA modification and protein processing. These findings expand the candidate pool of susceptibility determinants at both gene and isoform levels and provide concrete molecular targets-protection of chloroplast integrity, precise calibration of cell-death circuits, and maintenance of flavonoid metabolic capacity-for breeding durable, broad-spectrum resistance to spot blotch.

Supplementary information

The online version contains supplementary material available at:

Supplementary Figures

Supplementary Table 1: Genetic analysis of resistance to Spot Blotch in wheat.

Supplementary Table 2: Preview of transcriptome sequencing results of ZS31(R) and ZS3(S) leaf tissues.

Supplementary Table 3: GO and KEGG enrichment analysis of ZS54 and ZS57 genes in the leaf (L), sheath (S), and glume (G).

Supplementary Table 4: Hub genes identified in the three modules.

Supplementary Table 5: All AS events in both ZS54 and ZS57.

Supplementary Table 6: GO and KEGG enrichment analysis of ZS31 (R) and ZS3 (S) genes in the leaf (L).

Supplementary Table 7: Primer of qRT-PCR.

Declarations

Abbreviations

A3: Alternative 3′ splice site; A5: Alternative 5′ splice site; AF: Alternative first exon; AL: Alternative last exon; APA: Alternative polyadenylation; AS: Alternative splicing**;** BP: Biological process; CC: Cellular component; CDS: Coding sequence; DEGs: Differentially expressed genes; GO: Gene Ontology; GSEA: Gene Set Enrichment Analysis; HR: Hypersensitive response; KEGG: Kyoto Encyclopedia of Genes and Genomes; MF: Molecular function; MAPK: Mitogen-activated protein kinase; MX: Mutually exclusive exon; ONT: Oxford Nanopore full-length transcriptome; PACs:

Poly(A) sites; PCA: Principal component analysis; qRT-PCR: Quantitative real-time reverse transcription PCR; RI: Intron retention; ROS: Reactive oxygen species; SE: exon skipping; TCA: Tricarboxylic acid; TOM: Topological overlap matrix**;** WGCNA: Weighted gene co-expression network analysis.

Ethics approval and consent to participate Not applicable.

Consent for publication Not applicable.

Availability of data and materials All data supporting the findings of this study are available within the paper and within its supplementary information published online. The raw sequencing data (ONT full-length transcriptome data) generated in this study have been deposited in the Genome Sequence Archive (GSA) at the National Genomics Data Center (NGDC), China National Center for Bioinformation (CNCB) (https://ngdc.cncb.ac.cn/gsa/) under BioProject accession number [PRJCA080054] (GSA accession number: pending assignment; Submission ID: subCRA087863). The final GSA accession numbers will be provided and updated in the manuscript prior to publication.

Competing interests The authors declare no competing interests.

Funding

This work was supported by the Key Research and Development Program of Shandong Province [Grant No. 2024CXPT072-1].

Authors' contributions

Xingfeng Li conceived and designed the experiments, contributed reagents, materials, analysis tools, or data. Yinguang Bao and Haitao Cui provided technical assistance.

Chunting Wang and Yuanrui Zhu conducted the investigation. Jian Shen provided drawing assistance. Xinyu Wan analyzed and interpreted the data. Shuang Liang conceived and designed the experiments; performed the experiments; analyzed and interpreted the data; contributed reagents, materials, analysis tools, or data; and wrote the paper. All authors approved the final manuscript.

Acknowledgements

We are particularly grateful to Professor Zhiyong Liu, Institute of Genetics and Developmental Biology, Chinese Academy of Sciences, for his guidance and assistance.

References

1. Ma Z, Xie Q, Li G, Jia H, Zhou J, Kong Z, et al. Germplasms, genetics and genomics for better control of disastrous wheat Fusarium head blight. Theor Appl Genet. 2020;133:1541–68. https://doi.org/10.1007/s00122-019-03525-8.

2. Figueroa M, Hammond-Kosack KE, Solomon PS. A review of wheat diseases-a field perspective. Mol Plant Pathol. 2018;19:1523–36. https://doi.org/10.1111/mpp.12618.

3. Singh RP, Singh PK, Rutkoski J, Hodson DP, He X, Jørgensen LN, et al. Disease Impact on Wheat Yield Potential and Prospects of Genetic Control. Annu Rev Phytopathol. 2016;54:303–22. https://doi.org/10.1146/annurev-phyto-080615-095835.

4. Roy C, He X, Gahtyari NC, Mahapatra S, Singh PK. Managing spot blotch disease in wheat: Conventional to molecular aspects. Front Plant Sci. 2023;14:1098648. https://doi.org/10.3389/fpls.2023.1098648.

5. Yadav S, Raazi Z, Shivaraj SM, Somani D, Prashant R, Kulkarni A, et al. Whole Genome Sequencing and Comparative Genomics of Indian Isolates of Wheat Spot

858 Blotch Pathogen *Bipolaris sorokiniana* Reveals Expansion of Pathogenicity Gene
859 Clusters. Pathogens. 2022;12:1. https://doi.org/10.3390/pathogens12010001.
860 6. Chakraborty S, Mahapatra S, Hooi A, Bhushan BT, Almansour MI, Ansari MJ, et al.
861 Survey, isolation and characterisation of *Bipolaris sorokiniana* (Shoem.) causing spot
862 blotch disease in wheat under the climatic conditions of the Indo–Gangetic plains of
863 India. Heliyon. 2024;10:e40398. https://doi.org/10.1016/j.heliyon.2024.e40398.
864 7. Farzana L, Islam SS, Rahman M, Ferdus H, Hossain MdM. Addressing *Bipolaris*
865 *sorokiniana* in wheat: challenges, management strategies, and future directions for
866 sustainable food security. Discov Agric. 2025;3:211. https://doi.org/10.1007/s44279-
867 025-00389-z.
868 8. Lillemo M, Joshi AK, Prasad R, Chand R, Singh RP. QTL for spot blotch resistance
869 in bread wheat line Saar co-locate to the biotrophic disease resistance loci *Lr34* and
870 *Lr46*. Theor Appl Genet. 2013;126:711–9. https://doi.org/10.1007/s00122-012-2012-6.
871 9. Kumar S, Röder MS, Tripathi SB, Kumar S, Chand R, Joshi AK, et al. Mendelization
872 and fine mapping of a bread wheat spot blotch disease resistance QTL. Mol Breeding.
873 2015;35:218. https://doi.org/10.1007/s11032-015-0411-5.
874 10. Kumar S, Röder MS, Singh RP, Kumar S, Chand R, Joshi AK, et al. Mapping of
875 spot blotch disease resistance using NDVI as a substitute to visual observation in wheat
876 (*Triticum aestivum L.*). Mol Breeding. 2016;36:95. https://doi.org/10.1007/s11032-
877 016-0515-6.
878 11. Lu P, Liang Y, Li D, Wang Z, Li W, Wang G, et al. Fine genetic mapping of spot
879 blotch resistance gene *Sb3* in wheat (*Triticum aestivum*). Theor Appl Genet.

880 2016;129:577–89. https://doi.org/10.1007/s00122-015-2649-z.
881 12. Zhang P, Guo G, Wu Q, Chen Y, Xie J, Lu P, et al. Identification and fine mapping
882 of spot blotch (*Bipolaris sorokiniana*) resistance gene *Sb4* in wheat. Theor Appl Genet.
883 2020;133:2451–9. https://doi.org/10.1007/s00122-020-03610-3.
884 13. Li B, Xie J, Guo G, Zhang P, Zhang H, Zhu K, et al. Two independent dominant
885 resistance genes confer resistance to spot blotch in wheat. Theor Appl Genet.
886 2026;139:303. https://doi.org/10.1007/s00122-026-05412-5.
887 14. Navathe S, Yadav PS, Chand R, Mishra VK, Vasistha NK, Meher PK, et al. *ToxA–*
888 *Tsn1* Interaction for Spot Blotch Susceptibility in Indian Wheat: An Example of Inverse
889 Gene-for-Gene Relationship. Plant Disease. 2020;104:71–81.
890 https://doi.org/10.1094/PDIS-05-19-1066-RE.
891 15. Ayana GT, Ali S, Sidhu JS, Gonzalez Hernandez JL, Turnipseed B, Sehgal SK.
892 Genome-Wide Association Study for Spot Blotch Resistance in Hard Winter Wheat.
893 Front Plant Sci. 2018;9:926. https://doi.org/10.3389/fpls.2018.00926.
894 16. Singh PK, He X, Sansaloni CP, Juliana P, Dreisigacker S, Duveiller E, et al.
895 Resistance to Spot Blotch in Two Mapping Populations of Common Wheat Is
896 Controlled by Multiple QTL of Minor Effects. International Journal of Molecular
897 Sciences. 2018;19:4054. https://doi.org/10.3390/ijms19124054.
898 17. Bainsla NK, Phuke RM, He X, Gupta V, Bishnoi SK, Sharma RK, et al. Genome-
899 wide association study for spot blotch resistance in Afghan wheat germplasm. Plant
900 Pathology. 2020;69:1161–71. https://doi.org/10.1111/ppa.13191.
901 18. Yuan M, Zeng Q, Hua L, Chen S, Wu J, Zhao S, et al. Wheat *TaNADPO* Promotes

902 Spot Blotch Resistance. Mol Plant Pathol. 2025;26:e70103.
903 https://doi.org/10.1111/mpp.70103.
904 19. Gorash A, Armonienė R, Kazan K. Can effectoromics and loss-of-susceptibility be
905 exploited for improving Fusarium head blight resistance in wheat? The Crop Journal.
906 2021;9:1–16. https://doi.org/10.1016/j.cj.2020.06.012.
907 20. Li S, Lin D, Zhang Y, Deng M, Chen Y, Lv B, et al. Genome-edited powdery mildew
908 resistance in wheat without growth penalties. Nature. 2022;602:455–60.
909 https://doi.org/10.1038/s41586-022-04395-9.
910 21. Leng Y, Kümmel F, Zhao M, Molnár I, Doležel J, Logemann E, et al. A barley MLA
911 immune receptor is activated by a fungal nonribosomal peptide effector for disease
912 susceptibility. New Phytologist. 2025;245:1197–215.
913 https://doi.org/10.1111/nph.20289.
914 22. Jin Y, Li W, Li Y, Li D, Yan H, Chen S, et al. Pm37 as a susceptible Sr22 allele
915 confers resistance to wheat powdery mildew and leaf rust. Nat Commun. 2026;17:3165.
916 https://doi.org/10.1038/s41467-026-69717-1.
917 23. Wang N, Tang C, Fan X, He M, Gan P, Zhang S, et al. Inactivation of a wheat protein
918 kinase gene confers broad-spectrum resistance to rust fungi. Cell. 2022;185:2961-
919 2974.e19. https://doi.org/10.1016/j.cell.2022.06.027.
920 24. Faris JD, Zhang Z, Lu H, Lu S, Reddy L, Cloutier S, et al. A unique wheat disease
921 resistance-like gene governs effector-triggered susceptibility to necrotrophic pathogens.
922 Proceedings of the National Academy of Sciences. 2010;107:13544–9.
923 https://doi.org/10.1073/pnas.1004090107.

924 25. Schie CCN van, Takken FLW. Susceptibility Genes 101: How to Be a Good Host.
925 Annual Review of Phytopathology. 2014;52 Volume 52, 2014:551–81.
926 https://doi.org/10.1146/annurev-phyto-102313-045854.
927 26. Langfelder P, Horvath S. WGCNA: an R package for weighted correlation network
928 analysis. BMC Bioinformatics. 2008;9:559. https://doi.org/10.1186/1471-2105-9-559.
929 27. Kabbage M, Yarden O, Dickman MB. Pathogenic attributes of *Sclerotinia*
930 *sclerotiorum*: Switching from a biotrophic to necrotrophic lifestyle. Plant Science.
931 2015;233:53–60. https://doi.org/10.1016/j.plantsci.2014.12.018.
932 28. Jia J, Lu W, Liu B, Fang H, Yu Y, Mo W, et al. An atlas of plant full-length RNA
933 reveals tissue-specific and monocots–dicots conserved regulation of poly(A) tail length.
934 Nat Plants. 2022;8:1118–26. https://doi.org/10.1038/s41477-022-01224-9.
935 29. Tu Z, Shen Y, Wen S, Zong Y, Li H. Alternative Splicing Enhances the
936 Transcriptome Complexity of Liriodendron chinense. Front Plant Sci. 2020;11.
937 https://doi.org/10.3389/fpls.2020.578100.
938 30. Singh RM, Urmila. Spot blotch pathogens revisited: taxonomic insights and
939 resistance strategies in wheat—a mini review. Discov Plants. 2026;3:208.
940 https://doi.org/10.1007/s44372-026-00605-0.
941 31. Kangasjärvi S, Neukermans J, Li S, Aro E-M, Noctor G. Photosynthesis,
942 photorespiration, and light signalling in defence responses. J Exp Bot. 2012;63:1619–
943 36. https://doi.org/10.1093/jxb/err402.
944 32. Nomura H, Komori T, Uemura S, Kanda Y, Shimotani K, Nakai K, et al.
945 Chloroplast-mediated activation of plant immune signalling in Arabidopsis. Nat

946 Commun. 2012;3:926. https://doi.org/10.1038/ncomms1926.
947 33. Serrano I, Audran C, Rivas S. Chloroplasts at work during plant innate immunity. J
948 Exp Bot. 2016;67:3845–54. https://doi.org/10.1093/jxb/erw088.
949 34. de Torres Zabala M, Littlejohn G, Jayaraman S, Studholme D, Bailey T, Lawson T,
950 et al. Chloroplasts play a central role in plant defence and are targeted by pathogen
951 effectors. Nature Plants. 2015;1:15074. https://doi.org/10.1038/nplants.2015.74.
952 35. Winkel-Shirley B. Biosynthesis of flavonoids and effects of stress. Current Opinion
953 in Plant Biology. 2002;5:218–23. https://doi.org/10.1016/S1369-5266(02)00256-X.
954 36. Kimura M, Yamamoto YY, Seki M, Sakurai T, Sato M, Abe T, et al. Identification
955 of Arabidopsis Genes Regulated by High Light–Stress Using cDNA Microarray.
956 Photochemistry and Photobiology. 2003;77:226–33. https://doi.org/10.1562/0031-
957 8655(2003)0770226IOAGRB2.0.CO2.
958 37. Walia H, Wilson C, Condamine P, Liu X, Ismail AM, Zeng L, et al. Comparative
959 transcriptional profiling of two contrasting rice genotypes under salinity stress during
960 the vegetative growth stage. PLANT PHYSIOL. 2005;139:822–35.
961 https://doi.org/10.1104/pp.105.065961.
962 38. Mierziak J, Kostyn K, Kulma A. Flavonoids as Important Molecules of Plant
963 Interactions with the Environment. Molecules. 2014;19:16240–65.
964 https://doi.org/10.3390/molecules191016240.
965 39. Xu W, Xu X, Han R, Wang X, Wang K, Qi G, et al. Integrated transcriptome and
966 metabolome analysis reveals that flavonoids function in wheat resistance to powdery
967 mildew. Front Plant Sci. 2023;14. https://doi.org/10.3389/fpls.2023.1125194.

968 40. Berger S, Sinha AK, Roitsch T. Plant physiology meets phytopathology: plant
969 primary metabolism and plant–pathogen interactions. J Exp Bot. 2007;58:4019–26.
970 https://doi.org/10.1093/jxb/erm298.
971 41. Bilgin DD, Zavala JA, Zhu J, Clough SJ, Ort DR, DeLUCIA EH. Biotic stress
972 globally downregulates photosynthesis genes. Plant, Cell & Environment.
973 2010;33:1597–613. https://doi.org/10.1111/j.1365-3040.2010.02167.x.
974 42. Bolton MD. Primary Metabolism and Plant Defense—Fuel for the Fire. MPMI.
975 2009;22:487–97. https://doi.org/10.1094/MPMI-22-5-0487.
976 43. Voll LM, Zell MB, Engelsdorf T, Saur A, Wheeler MG, Drincovich MF, et al. Loss
977 of cytosolic NADP-malic enzyme 2 in Arabidopsis thaliana is associated with enhanced
978 susceptibility to Colletotrichum higginsianum. New Phytologist. 2012;195:189–202.
979 https://doi.org/10.1111/j.1469-8137.2012.04129.x.
980 44. Morkunas I, Ratajczak L. The role of sugar signaling in plant defense responses
981 against fungal pathogens. Acta Physiol Plant. 2014;36:1607–19.
982 https://doi.org/10.1007/s11738-014-1559-z.
983 45. Ye W, Liu T, Zhang W, Li S, Zhu M, Li H, et al. Disclosure of the Molecular
984 Mechanism of Wheat Leaf Spot Disease Caused by Bipolaris sorokiniana through
985 Comparative Transcriptome and Metabolomics Analysis. International Journal of
986 Molecular Sciences. 2019;20:6090. https://doi.org/10.3390/ijms20236090.
987 46. Ahuja I, Kissen R, Bones AM. Phytoalexins in defense against pathogens. Trends
988 in Plant Science. 2012;17:73–90. https://doi.org/10.1016/j.tplants.2011.11.002.
989 47. Rojas CM, Senthil-Kumar M, Tzin V, Mysore K. Regulation of primary plant

990 metabolism during plant-pathogen interactions and its contribution to plant defense.
991 Front Plant Sci. 2014;5. https://doi.org/10.3389/fpls.2014.00017.
992 48. Winter G, Todd CD, Trovato M, Forlani G, Funck D. Physiological implications of
993 arginine metabolism in plants. Front Plant Sci. 2015;6.
994 https://doi.org/10.3389/fpls.2015.00534.
995 49. Glagoleva AY, Vikhorev AV, Shmakov NA, Morozov SV, Chernyak EI, Vasiliev GV,
996 et al. Features of Activity of the Phenylpropanoid Biosynthesis Pathway in Melanin-
997 Accumulating Barley Grains. Front Plant Sci. 2022;13.
998 https://doi.org/10.3389/fpls.2022.923717.
999 50. Liu X, Liu H, Tian B, Shi G, Liu C, Guo J, et al. Metabolome and transcriptome
1000 analyses of anthocyanin biosynthesis reveal key metabolites and candidate genes in
1001 purple wheat (Triticum aestivum L.). Physiologia Plantarum. 2023;175:e13921.
1002 https://doi.org/10.1111/ppl.13921.
1003 51. Morel J-B, Dangl JL. The hypersensitive response and the induction of cell death
1004 in plants. Cell Death Differ. 1997;4:671–83. https://doi.org/10.1038/sj.cdd.4400309.
1005 52. Govrin EM, Levine A. The hypersensitive response facilitates plant infection by the
1006 necrotrophic pathogen *Botrytis cinerea*. Current Biology. 2000;10:751–7.
1007 https://doi.org/10.1016/S0960-9822(00)00560-1.
1008 53. Glazebrook J. Contrasting Mechanisms of Defense Against Biotrophic and
1009 Necrotrophic Pathogens. Annual Review of Phytopathology. 2005;43 Volume 43,
1010 2005:205–27. https://doi.org/10.1146/annurev.phyto.43.040204.135923.
1011 54. Kumar J, Schäfer P, Hückelhoven R, Langen G, Baltruschat H, Stein E, et al.

1012 *Bipolaris sorokiniana*, a cereal pathogen of global concern: cytological and molecular
1013 approaches towards better control‡. Mol Plant Pathol. 2002;3:185–95.
1014 https://doi.org/10.1046/j.1364-3703.2002.00120.x.
1015 55. Torres MA, Jones JDG, Dangl JL. Reactive Oxygen Species Signaling in Response
1016 to Pathogens. Plant Physiol. 2006;141:373–8. https://doi.org/10.1104/pp.106.079467.
1017 56. Jones JDG, Dangl JL. The plant immune system. Nature. 2006;444:323–9.
1018 https://doi.org/10.1038/nature05286.
1019 57. Gupta PK, Chand R, Vasistha NK, Pandey SP, Kumar U, Mishra VK, et al. Spot
1020 blotch disease of wheat: the current status of research on genetics and breeding. Plant
1021 Pathology. 2018;67:508–31. https://doi.org/10.1111/ppa.12781.
1022 58. Basak P, Gurjar MS, Kumar TPJ, Kashyap N, Singh D, Jha SK, et al. Transcriptome
1023 analysis of *Bipolaris sorokiniana* - *Hordeum vulgare* provides insights into mechanisms
1024 of host-pathogen interaction. Front Microbiol. 2024;15:1360571.
1025 https://doi.org/10.3389/fmicb.2024.1360571.
1026 59. Audenaert K, Meyer GBD, Höfte MM. Abscisic Acid Determines Basal
1027 Susceptibility of Tomato to Botrytis cinerea and Suppresses Salicylic Acid-Dependent
1028 Signaling Mechanisms. Plant Physiology. 2002;128:491–501.
1029 60. Rose JKC, Braam J, Fry SC, Nishitani K. The XTH Family of Enzymes Involved
1030 in Xyloglucan Endotransglucosylation and Endohydrolysis: Current Perspectives and a
1031 New Unifying Nomenclature. Plant Cell Physiol. 2002;43:1421–35.
1032 https://doi.org/10.1093/pcp/pcf171.
1033 61. Anderson JP, Badruzsaufari E, Schenk PM, Manners JM, Desmond OJ, Ehlert C, et

al. Antagonistic Interaction between Abscisic Acid and Jasmonate-Ethylene Signaling Pathways Modulates Defense Gene Expression and Disease Resistance in Arabidopsis. Plant Cell. 2004;16:3460–79. https://doi.org/10.1105/tpc.104.025833.

62. Fan J, Hill L, Crooks C, Doerner P, Lamb C. Abscisic Acid Has a Key Role in Modulating Diverse Plant-Pathogen Interactions. Plant Physiol. 2009;150:1750–61. https://doi.org/10.1104/pp.109.137943.

63. Bellincampi D, Cervone F, Lionetti V. Plant cell wall dynamics and wall-related susceptibility in plant–pathogen interactions. Front Plant Sci. 2014;5. https://doi.org/10.3389/fpls.2014.00228.

64. Barkan A, Small I. Pentatricopeptide Repeat Proteins in Plants. Annual Review of Plant Biology. 2014;65:415–42. https://doi.org/10.1146/annurev-arplant-050213-040159.

65. Saracco SA, Miller MJ, Kurepa J, Vierstra RD. Genetic Analysis of SUMOylation in Arabidopsis: Conjugation of SUMO1 and SUMO2 to Nuclear Proteins Is Essential. Plant Physiol. 2007;145:119–34. https://doi.org/10.1104/pp.107.102285.

66. DIELEN A, BADAOUI S, CANDRESSE T, GERMAN-RETANA S. The ubiquitin/26S proteasome system in plant–pathogen interactions: a never-ending hide-and-seek game. Mol Plant Pathol. 2009;11:293–308. https://doi.org/10.1111/j.1364-3703.2009.00596.x.

67. Adams EHG, Spoel SH. The ubiquitin–proteasome system as a transcriptional regulator of plant immunity. Journal of Experimental Botany. 2018;69:4529–37. https://doi.org/10.1093/jxb/ery216.

1056 68. Ament IH, DeBruyne N, Wang F, Lin L. Long-read RNA sequencing: A
1057 transformative technology for exploring transcriptome complexity in human diseases.
1058 Mol Ther. 2025;33:883–94. https://doi.org/10.1016/j.ymthe.2024.11.025.

Supplementary Files

This is a list of supplementary files associated with this preprint. Click to download.

- SupplementalFigures.pdf
- SupplementalTable12457.xlsx
- SupplementalTable6.xlsx
- SupplementalTable3.xlsx